Pressure-induced $B1$-$B2$ phase transition in alkali halides: General aspects from first-principles calculations

A. Martín Pendás, V. Luaña, J. M. Recio, M. Flórez, E. Francisco, M. A. Blanco, and L. N. Kantorovich*

Departamento de Química Física y Analítica, Universidad de Oviedo, 33006 Oviedo, Spain

(Received 2 August 1993; revised manuscript received 27 September 1993)

A first principles, general study of the thermodynamic and kinetic aspects of the $B1$-$B2$ phase transition in alkali halides is presented. Particular attention is paid to (a) how to construct models of increasing complexity to be used with generic quantum-chemistry techniques and (b) the topological and symmetry-dependent features of the energetic and the Gibbs potential surfaces analyzed. Our results indicate that the transition may be thought of as involving the simultaneous opening of the rhombohedral angle in the primitive $B1$ crystallographic cell while a contraction of the lattice parameter takes place. Transition paths depend strongly on pressure and show large and asymmetric Gibbs barriers that qualitatively account for many of the empirical facts around the phenomenon of hysteresis.

I. INTRODUCTION

The alkali halides have been, due to their simplicity, the preferred model systems in which new theories and experimental methodologies have been validated since the advent of solid-state theory. Their thermodynamic, elastic, structural, and defect properties have been widely investigated[1] for over 70 years, and are well understood. These compounds generally crystallize in either the $B1$ (NaCl-type), or the $B2$ (CsCl-type) structures, and are known to undergo pressure- and temperature-induced first-order transitions, as described by the seminal work of Slater.[2] Among them, the $B1$ to $B2$ pressure-induced transition shown by many of the systems that exist in the $B1$ phase at zero pressure is the best documented one,[3] standing as one of the simplest nondisplacive first-order transitions known. There is a considerable interest in the understanding of the energetic and dynamic features of the mechanism of this transformation, as it involves the concerted and cooperative movement of a large number of atoms and may be taken as a model for other solid-solid transformations of great geological and planetary importance.[4]

A large amount of experimental work has been done in the last two decades along this direction, and a good deal of thermodynamic and some kinetic data have been gathered. A critical survey of the available information shows that the kinetics is extremely sensitive to a big number of variables such as the purity and the previous thermal and mechanical treatments of the sample under investigation,[5] the rate of increase of pressure, the pressure gradient across the crystal or its grain structure,[6] etc. This fact precludes the extraction of meaningful, general information about the transition dynamics. Some of the studies have been primarily interested in the hysteresis phenomena. The transition is not thermodynamically reversible in laboratory conditions: a pressure higher than the thermodynamic phase transition pressure is necessary to obtain the $B2$ phase when increasing the

pressure of a $B1$ crystal and a lower pressure when going in the opposite direction. The complete experiment covering direct and reverse transitions constitutes a hysteresis cycle and the pressure range between the $B1 \rightarrow B2$ and the $B2 \rightarrow B1$ transformations the hysteresis range. It seems well established that the qualitative features of the hystereis range depend reproducibly on the variables commented above.[5] The hysteresis range is greater in pure or thermally treated crystals and in the first hysteresis cycle. It increases abruptly with decreasing cation size when examining a series of compounds. The hysteresis range also decreases almost exponentially with increasing temperature, and becomes greater when the pressure is changed suddenly. All these evidences point towards the existence of large energetic barriers that must be surmounted in the transition mechanism.

Basically, two successful models have been used to explain the transformation. The first one, initially proposed by Shoji[7] and later modified by Buerger[8] suggests a contraction along one of the threefold axes. The second was put forward by Watanabe, Tokonami, and Morimoto[9] (WTM) after observing orientational relations among crystallographic directions in initial ($B2$) and final ($B1$) phases of CsCl undergoing a temperature-induced transformation. It consists of a highly concerted intralayer rearrangement of atoms associated with interlayer translations.

On the other hand, while a lot of calculations have been published predicting the thermodynamic transition pressure, very little work has been done on the kinetic and mechanistic aspects of the phenomenon. This fact emanates from what has been called "the crystal stability problem:" it is very difficult to predict the structure that a particular system exhibits for a given set of conditions and even more difficult to assess the relative stability of two energetically similar phases. Any theoretical investigation addressing the $B1$-$B2$ transition mechanism should rely upon a method with a positive answer to this first problem. The vast majority of the theoretical analyses

have tried to correctly predict the thermodynamic transition pressures using several techniques ranging from pair potentials[10] to density-functional[11] or *ab initio*[12] models. Regarding the mechanism of the transition or the hysteresis phenomena and, as far as we know, every theoretical attempt along this line has been based on some kind of pairwise simulation. Nakagiri and Nomura[13] used Born-Mayer potentials supplemented with several van der Waals terms to predict the existence of a barrier in the WTM model. Ruff *et al.*[14] applied isothermal-isobaric molecular dynamics with Tosi-Fumi[15] potentials to discard Buerger's mechanism and confirm the WTM one. Their simulation was, however, extremely sensitive to simulation parameters and the predicted transition pressures computed tenths of times greater than experiment. Nga and Ong[16] used also isothermal-isobaric and Parrinello-Rahman molecular dynamics with Tosi-Fumi potentials to conclude that both Buerger and WTM were essentially equivalent. Their predicted transition pressures were also many times greater than the observed values. Due to the shortcomings associated with the use of empirical or semiempirical pair potentials in thermodynamic conditions far from those used to generate them,[17] and given the actual problems in achieving realistic size in isothermal-isobaric molecular-dynamics simulations, we think that there is a deep demand of rigorous, quantum-mechanical results that may open the way to further studies.

It is the purpose of this paper to present a general scope first-principles study of the $B1$-$B2$ phase-transition thermodynamics and dynamics. The method used has been the *ab initio* perturbed ion model (AIPI),[18,19(a),19(b)] a successful scheme in the prediction of both quantitative thermodynamic data for a wide class of crystals and trends along families of related compounds. We will focus on the techniques used and on how to get physical insight into the global characteristics of the transition. Particular results will be discussed for a model system, the LiCl crystal. A full quantitative and comparative discussion of the features here analyzed on the whole alkali halides series will be published elsewhere.

The paper is organized as follows. In Sec. II, we will briefly comment on the method employed and summarize some thermodynamic results on the alkali halides. Section III will be devoted to the transition mechanism and its static (zero temperature, no zero-point contributions) *ab initio* modeling. This issue is followed by a discussion of the information contained in the energy and Gibbs potential surfaces and their topological features (Sec. IV). In Sec. V we will try to throw some light on the transition path and the origin of the hysteresis range and other experimental kinetic behaviors from our first-principles point of view and, finally, we will summarize our results and comment some perspectives in Sec. VI.

II. METHOD

The *ab initio* perturbed ion method[18,19(a),19(b)] is a first-principles approach to the construction of the electronic structure of weakly overlapping pure and defective solids. Its foundation lies in the theory of electronic

separability[20] for weakly overlapping groups[21] and in the Adams-Gilbert formalism.[22,23] It solves the Hartree-Fock (HF) equations of the solid in a localized Fock space by breaking the crystal wave function into local nearly orthogonal group functions (atomic or ionic in nature). At the end of a self-consistent process we get the total energy of the system and a set of completely localized wave functions for every crystallographically nonequivalent atom or ion. These local functions may be used to study the change in nature of the crystal constituents on going from the gas phase to the solid or to reconstruct the band structure by rotating to the canonical HF solution.

The localized nature of the AIPI procedure has for our purposes a number of advantages over the usual canonical approach:[24] (a) A localized picture is much better suited to incorporate several degrees of approximations in order to solve the equations. This has allowed the construction of a very efficient algorithm using the nearly HF multizeta exponential (Slater-type orbital) Clementi and Roetti basis sets.[25] (b) With a localized solution it is easy and fruitful to divide the total energy of the system into atomic (ionic) and interatomic (interionic) contributions. The latter may be further used to obtain crystal adapted pair potentials.[17] (c) As in weakly overlapping solids the correlation energy correction is almost entirely intra-atomic in nature (being therefore a sum of contributions from every group), localized wave functions may be exploited to attain size consistent good estimations of this correction. In the present implementation of the AIPI code, the correlation energy correction is obtained through Clementi's Coulomb-Hartree-Fock method.[26]

As far as the alkali halides are concerned, the method has been proved to be a valuable predictive tool in thermodynamic studies. In a previous paper[27] we have reported thermochemical, elastic, and p-V static data in almost quantitative agreement with the experimental values.[5,6,13,28-35] In Table I we gather some of these results. Static transition pressures have been obtained in the thermodynamic limit by solving for the pressure that makes equal the Gibbs potentials of both phases:

$$G_{B1}(T=0)=U_{B1}+p_{tr}V_{B1}$$
$$=G_{B2}(T=0)=U_{B2}+p_{tr}V_{B2} , \qquad (1)$$

where U is the total computed energy of the crystal at each volume. Note that there has not yet been found an experimental $B1$-$B2$ transition in LiCl, while the AIPI value for this system lies around 80 GPa. This is the fundamental reason to take this system as our model in this general paper.

As stated in the Introduction, it is the overall agreement with experimental trends that gives us confidence in obtaining reliable results when exploring the transition mechanism. This condition should always be borne in mind in theoretical investigations on phase transitions.

The rest of the paper will be based on AIPI calculations made with Clementi and Roetti's basis sets, the Coulomb-Hartree-Fock method for the estimation of the correlation energy correction, and a convergence in the crystal total energies better than 10^{-8} Hartree. This

TABLE I. Cohesive and thermodynamic transition phase data for the alkali chlorides. R_0 stands for the first-neighbor distance, E_{latt} for the lattice energy, B_0 for the zero-pressure isothermal bulk modulus, P_{tr} for the thermodynamic transition pressure, V_{tr} for the molar volume at the transition point, and HR for the hysteresis range. Theoretical values obtained after AIPI computations (Ref. 27).

		LiCl	NaCl	KCl	RbCl	CsCl
R_0 (Å)	B1	2.591	2.800	3.267	3.391	3.366
	B2	2.828	2.975	3.385	3.459	3.407
	Expt.	2.539[a]	2.789[a]	3.116[a]	3.259[a]	3.571[b]
E_{latt}	B1	−200.8	−189.6	−163.1	−159.5	−161.0
(kcal/mol)	B2	−183.1	−178.8	−160.5	−159.2	−166.0
	Expt.	−202[c]	−185[c]	−170[c]	−162[c]	−155.1[d]
B_0 (GPa)	B1	31.2	28.8	15.5	15.3	10.0
	B2	24.1	25.6	19.6	19.3	12.5
	Expt.	35.5[e]	28.5[e]	20.2[e]	18.5[e]	16.6[f]
P_{tr} (GPa)	Theor.	~80	22	2	0.2	
	Expt.		26[g]	2[i]	0.5[i]	
$V_{tr}B1$	Theor.	10.3	18.6	37.9	45.6	
	Expt.		17.36[h]	34.35[i]	41.43[i]	
$V_{tr}B2$	Theor.	9.3	16.5	33.0	37.5	
	Expt.		16.37[h]	30.14[i]	35.38[i]	
HR (GPa)	Expt.		6.8[j]	0.5[k]	0.15[l]	

[a]Reference 28.
[b]Reference 29.
[c]Reference 30.
[d]Reference 31.
[e]Reference 32.
[f]Reference 33.

[g]Reference 6.
[h]Reference 34.
[i]Reference 35.
[j]Reference 6.
[k]Reference 13.
[l]Reference 5.

represents adding up quantum contributions to the interaction energies up to neighbors 30 bohr away from a chosen atom.

III. *AB INITIO* MODELING AND MECHANISM

The *ab initio* modeling of a solid-solid transformation, considered in the chemical sense of reaction as the movement of the system onto a high-dimensional potential-energy surface, is not an easy task given the huge number of degrees of freedom involved. It is then necessary to introduce some simplifying assumptions that, according to our point of view, and due to the controversial experimental and theoretical investigations on the transition mechanism, should be as wide as possible and should never discriminate some mechanisms in favor of others. These assumptions must also be constructed in a hierarchical and easy generalizable manner. We have undertaken such a program in an ordered way.

First, we assume that a continuous path on some high-dimensional (though not infinite dimensional) space exists connecting the B1 and B2 phases. This space will be called the transition configuration space. Assuming that the phase transition is an extremely cooperative and concerted process, it seems plausible to suppose perfect periodic lattices at each point of this space. It is true that there are both experimental[5] and theoretical[14] evidences indicating a very important role of defects in the kinetics of the transition, but it is also certain that in its absence the reaction keeps taking place through even more concerted paths.

As the second step, we must now decide the number of crystallographically nonequivalent ions per primitive unit cell. This choice sets up our hierarchy of models. In this way, the simplest possible model is that in which there is only one different cation and one different anion remaining translationally invariant to every other during the transformation. Without loss of generality, we can set the crystallographic coordinates of the cation equal to (0,0,0) and leave the anion position float into the interior of the cell (x,y,z). We have then nine parameters: three of them coming from the (x,y,z), and the other six from the sizes and angles of the primitive unit cell $(a,b,c,\alpha,\beta,\gamma)$. This is the nine-dimensional (9D) transition configuration space model or, in brief, the 9D model. Both the B1 and B2 phases lie at particular points of the 9D transition configuration space:

$$-B1: \quad a=b=c, \quad \alpha=\beta=\gamma=60°, \quad x=y=z=\tfrac{1}{2},$$

$$-B2: \quad a=b=c, \quad \alpha=\beta=\gamma=90°, \quad x=y=z=\tfrac{1}{2},$$

and all our discussions will refer to it from now on. It is straightforward to increase the complexity (dimensionality) of such class of models, each new pair of nonequivalent ions adding six dimensions to the transition configuration space.

Despite being our simplest model, a 9D hypersurface is very hard to explore by *ab initio* methodologies, even in small molecules. Fortunately, symmetry can play a very important role in the simplification of the problem. It is well known from perturbative arguments[36] that if a nondegenerate chemical system does not leave its fundamental state electronic surface during the course of a transformation, the reaction coordinate must belong to the to-

tally symmetric representation of the point group at each point of the path with a nonzero energy gradient. As a corollary, once a system starts on a given reaction path, it must maintain the same point group symmetry along it until a zero-gradient energy point (critical point) is found (usually a transition state). As usual,[37] a system enters a reaction path from a critical point along the direction of minimum energy increase. Though it is possible to argue against electronically adiabatic phase transitions at constant pressure, it is extremely difficult to make actual calculations releasing that constraint, and we will not do it.

We have begun our modeling of the transition by taking fully into account the symmetry restrictions to the path just commented. Starting from one-parameter minimum energy optimized structures for the $B1$ and $B2$ crystals (note that due to cubic symmetry the lattice spacing is the only free parameter in the two phases), we have numerically constructed and diagonalized the (9×9) Hessian matrix of the total energy at both configurations. Representative results for the LiCl crystal are shown in Table II, and will be further discussed in other sections. Qualitatively similar data are found for the other alkali halides. Our conclusions are highly significant. The minimum energy eigenvalue corresponds to a path starting in the direction $a = b = c$, $\alpha = \beta = \gamma$, $x = y = z = \frac{1}{2}$, with a definite ratio between the a and α movements. The highest symmetry compatible with these relations is

TABLE II. Properties of the energetically optimum $B1$ and $B2$ configurations onto the 9D $\{a,b,c,\alpha,\beta,\gamma,x,y,z\}$ surface. ∇_ω refers to the ω component of the energy gradient and $H_{\omega\omega'}$ to the $\omega\omega'$ component of the energy Hessian. ε_{min} and V_{min} are, respectively, the lowest eigenvalue of the (9×9) Hessian matrix and its associated eigenvector in the $\{a,b,c,\alpha,\beta,\gamma,x,y,z\}$ coordinates. Only the minimal set of derivatives is shown. All values in atomic units.

	$B1$	$B2$
a	6.918 933	6.177 646
∇_a	0.000 111 00	0.000 006 73
∇_α	0.000 003 12	0
∇_x	0	0
H_{aa}	0.81951	1.13749
H_{ab}	−0.04620	−0.28290
$H_{a\alpha}$	−0.06713	0
H_{ax}	0	0
H_{ay}	0	0
$H_{a\beta}$	0.20236	0
H_{ax}	0	0
H_{ay}	0	0
$H_{\alpha\alpha}$	0.48090	−0.34581
$H_{\alpha\beta}$	−0.06775	0
H_{xx}	0.15831	−0.00789
H_{xy}	0.09210	0
ε_{min}	0.12118	−0.34581[a]
V_{min}	$(a,a,a,b,b,b,0,0,0)$ $a = -0.302\,878^b$ $b = 0.491\,529^b$	$(0,0,0,1,0,0,0,0,0)$[a]

[a]Threefold degenerate. The eigenvectors follow the three angle directions. Only one of these eigenvectors is shown here.
[b]Symmetry fixed.

$R\bar{3}m$ and, therefore, the whole path must lie on this restriction of the 9D surface. Moreover, as the stoichiometry must be preserved, the inner position cannot be altered on an $R\bar{3}m$ path. The minimum energy transition path must lie then on a 2D surface: $u = a = b = c$, $v = \alpha = \beta = \gamma$. Under the restriction of only one different kind of each ion, we have arrived at a modified Buerger mechanism, and the transformation is viewed as the opening of the rhombohedral angles of the primitive $B1$ cell coupled to a simultaneous change in the lattice spacing (Fig. 1). Our arguments hold true when the Gibbs potential surface, and not the total-energy surface, is analyzed. Though we have not exhausted all possible periodic mechanisms, our study has a clear generality not exploited up to now. We think that the picture drawn so far is completely general and that other theoretical schemes could take advantage of it.

The 2D AIPI static total energy (U) and 0-K Gibbs potential $(G = U + pV)$ surfaces have been obtained for a 2500-point grid in the systems under investigation. This has been possible in a reasonable amount of time due to the computational performance of the AIPI scheme. As an example, the CPU time needed to calculate the total energy of the LiCl crystal at a point of the 9D surface was 64 s on a CONVEX C-120. Benchmark times for other machines are gathered in Fig. 4 of Ref. 19(b). In Fig. 2 we depict the U surface versus the lattice spacing and the rhombohedral angle. Two facts are indeed remarkable: (a) the $B1$ point is a true minimum both in the 2D and 9D surfaces (see also Table II); (b) the $B2$ structure is a saddle point (six positive eigenvalues and three negative ones), and in the 2D restriction is unstable with respect to the rhombohedral angle. Therefore, the $B2$ phase is not even metastable at zero pressure for LiCl, though this situation changes with the system studied and will change as external pressure is applied.

The 0-K Gibbs potential surface is easily constructed at each pressure by adding the pV term to the U surface. As p increases, the $B2$ phase is favored against the $B1$,
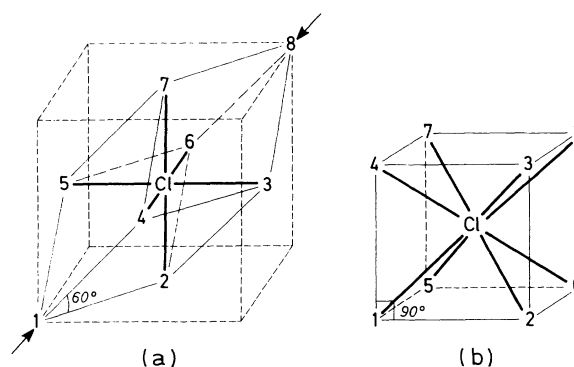

FIG. 1. Primitive $B1$ (a) and $B2$ (b) cells (P cells). The rhombohedral $B1$ cell is represented in relation to the usual face-centered cell (F cell). The arrows show the deformation of the $B1$ cell in Buerger's mechanism of the $B1$-$B2$ phase transition. Cationic sites are numbered in both cells in order to clarify the coordination relations during the transition. (After West, Ref. 42.)
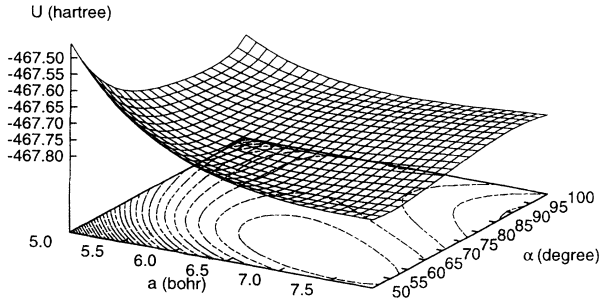
FIG. 2. Static total energy (U) 2D surface for the LiCl pure crystal according to AIPI calculations. The $B1$ and $B2$ configurations are shown as minimum and saddle points located at $\alpha = 60°$ and $\alpha = 90°$, respectively.

going from a saddle point to a minimum and eventually becoming more stable than the $B1$ structure.

IV. 2D SURFACE TOPOLOGY AND PHASE STABILITY

We have found that the main topological properties of the U and G surfaces, and subsequently of the transformation, are determined fundamentally by symmetry. One of the most important facts discovered is that both the $B1$ and $B2$ configurations turn out to be critical (null gradient) points of the Gibbs potential surface at every pressure examined, ranging from 0 to 300 GPa for LiCl. On increasing p, the $B2$ structure turns from a saddle to a degenerate point and then to a deeper and deeper minimum. Simultaneously, the $B1$ configuration suffers the reverse process. It is very interesting to clarify why these characteristics are symmetry determined.

To do so, let us introduce the well-known expansion of the crystal total energy in Lagrangian strain parameters, ε_{ik}, for a general homogeneous deformation of a crystalline solid around a fixed point:[38]

$$U = U_0 + U^{ik}\varepsilon_{ik} + \tfrac{1}{2}U^{ikjl}\varepsilon_{ik}\varepsilon_{jl} , \qquad (2)$$

where $\varepsilon_{ij} = \tfrac{1}{2}(g_{ij} - g_{ij}^0)$, g and g^0 being the metric tensors of the distorted and original unit cells. The contravariant character of the U^{ij} and U^{ikjl} coefficients as well as the covariant properties of ε_{ik} under coordinate changes is well known, and is the basis of our treatment. Establishing the connection between U derivatives with respect to cell parameters, $\{a_i\} = (a,b,c,\alpha,\beta,\gamma)$, and U derivatives with respect to Lagrangian strain parameters is an elementary task. Introducing now the Voigt components of Lagrangian strain parameters,

$$\varepsilon_1 = \varepsilon_{11} , \quad \varepsilon_2 = \varepsilon_{22} , \quad \varepsilon_3 = \varepsilon_{33} ,$$
$$\varepsilon_4 = 2\varepsilon_{23} , \quad \varepsilon_5 = 2\varepsilon_{13} , \quad \varepsilon_6 = 2\varepsilon_{12} , \qquad (3)$$

the matrix relating the a_i's and the Voigt components is easily obtained and will not be presented.

We can now pay particular attention to each of the two phases. As the $B2$ phase is concerned ($\alpha = \beta = \gamma = 90°$), we can derive the following relations:

$$\frac{\partial U}{\partial \varepsilon_i} = a_i^0 \frac{\partial U}{\partial a_i} \quad \{i = 1,2,3\} ,$$
$$\frac{\partial U}{\partial \varepsilon_i} = -\frac{\partial U}{\partial a_i} \quad \{i = 4,5,6\} , \qquad (4)$$

where (a^0, b^0, c^0) are the lattice parameters of the original cell.

The U^{ij} matrix [Eq. (2)] transforms contravariantly under coordinate changes, and must remain unchanged under the symmetry operations of the crystal. Applying all the symmetry operations of the O_h group we arrive at a simultaneous group of equalities that impose stringent restrictions on the possible values of the U^{ij} coefficients. Doing so, we verify that

$$\frac{\partial U}{\partial \alpha} = \frac{\partial U}{\partial \beta} = \frac{\partial U}{\partial \gamma} = 0, \quad \frac{\partial U}{\partial a} = \frac{\partial U}{\partial b} = \frac{\partial U}{\partial c} \neq 0 . \qquad (5)$$

As the argument only depends on cubic symmetry, the next statement follows: every cubic symmetry point must have null energy derivatives with respect to cubic angles.

In the $B1$ structure, the above relations still hold in the face-centered-cubic cell (F cell). However, in the rhombohedral primitive cell frame (P cell), the angle derivatives will certainly not be zero. It is, however, possible to convert the former to the latter using once again the transformation properties of the U^{ij} and the matrix relating the P-cell unit vectors to the F-cell ones.

Equating the derivatives of U with respect to angles in the F cell to zero, we obtain the attractive, nontrivial expression valid at every $B1$ point:

$$\frac{\partial U}{\partial \alpha} = \frac{\partial U}{\partial \beta} = \frac{\partial U}{\partial \gamma} = ka^0\frac{\partial U}{\partial a} = kb^0\frac{\partial U}{\partial b} = kc^0\frac{\partial U}{\partial c},$$
$$k = \frac{\sqrt{3}}{2} . \qquad (6)$$

It is perhaps interesting to remark that Eq. (6) was initially found as a not-easy-to-understand relation numerically satisfied by the two components of the energy gradient along the $\alpha = 60°$ line on analyzing our AIPI 2D total-energy surface. That "experimental" discovery inspired the above treatment.

Thus, the topological features of the energy are beautifully determined by symmetry constraints and boundary conditions. Let us summarize them. As regards boundary conditions, in the a-α space that we are considering, the Pauli principle forces the $\alpha = 0°$ and 120° lines to be infinite energy asymptotes, as both situations correspond to zero-volume cells. The same can be said of the $a = 0$ line. The $a = \infty$ region turns out to be a constant energy (free-ion energy) asymptotic plateau. Regarding symmetry restrictions, the $\alpha = 90°$ line is always a null gradient line, and the $\alpha = 60°$ line fulfills constant ratios between the two gradient components [Eq. (6)].

The characteristics of the 0-K G surface can now be ascertained and related to the thermodynamic phase stability problem. Introducing in its full form the molar volume into the static G function, we verify, after straightforward derivations, that both Eqs. (5) and (6) are also satisfied with G instead of U. The thermodynamically most stable configuration at a chosen p is that which

minimizes the Gibbs potential. When obtaining the optimum lattice parameter at every pressure for the $B1$ and $B2$ phases with conventional techniques [making $U+pV(a)$ minimum], Eqs. (5) and (6) assure that we are finding not only a critical point in the 1D a space, but also in the 2D a-α space. This conclusion is also generalizable to the general 9D surface. All optimum $B1$ or $B2$ points being critical points of the G function, how do their stabilities vary with pressure? To answer this question, we must explore the Hessian matrix of G and observe how its eigenvalues vary with p. This study is actually closely related to the elastic behavior of the crystal, as the elastic and effective elastic constants are generically defined as follows:

$$c^{ij} = \frac{1}{V} \frac{\partial^2 U}{\partial \varepsilon_i \partial \varepsilon_j} \, ,$$
$$c_{\text{eff}}^{ij} = \frac{1}{V} \frac{\partial^2 G}{\partial \varepsilon_i \partial \varepsilon_j} \, . \tag{7}$$

Due to the contravariant nature of the ε_i's, it is possible to relate these parameters to derivatives of the energy or the Gibbs potential with respect to the lattice parameters in the same way as done before.

For the $B2$ phase, the 2D Hessian of G at each optimum critical point acquires the subsequent simple structure:

$$H = \begin{vmatrix} \dfrac{\partial^2 G}{\partial u^2} & 0 \\ 0 & \dfrac{\partial^2 G}{\partial v^2} \end{vmatrix}$$
$$= \begin{vmatrix} 3\dfrac{\partial^2 U}{\partial a^2} + 6\dfrac{\partial^2 U}{\partial a\,\partial b} + 6ap & 0 \\ 0 & 3\dfrac{\partial^2 U}{\partial \alpha^2} + 6\dfrac{\partial^2 U}{\partial \alpha \partial \beta} - 3pa^3 \end{vmatrix} \, , \tag{8}$$

the crossed derivatives coming from the fact that in the 2D surface we assume $u=a=b=c$, $v=\alpha=\beta=\gamma$. Applying point group symmetry arguments to second derivatives of U similar to those previously used, it may be proven that the crossed angle derivative is zero at any cubic symmetry point. With Eq. (7), it follows that

$$H_{uu} = \frac{3V}{a^2}(c_{\text{eff}}^{11} + 2c_{\text{eff}}^{12}) \, ,$$
$$H_{vv} = 3Vc_{\text{eff}}^{44} \, , \tag{9}$$
$$c_{\text{eff}}^{11} = c^{11} - p, \quad c_{\text{eff}}^{12} = c^{12} + p, \quad c_{\text{eff}}^{44} = c^{44} - p \, .$$

The Hessian of G in the $B1$ phase is also connected to the effective elastic constants. It is first necessary to use Eq. (7) to obtain the elastic constants in the rhombohedral P cell and then transform them to the usual cubic F-cell frame by using their covariance properties. We can always look at Eqs. (8) and (9) as also referred to the $B1$ configurations if we remind the reader that a and α are now cubic parameters and not rhombohedral ones,

and that the volume term now involves $a^3/4$ instead of a^3.

Now we see how the nature of the $B1$ and $B2$ critical points onto the 2D Gibbs surface is altered on changing the pressure. The H_{uu} element (or, in other words, $c_{\text{eff}}^{11} + 2c_{\text{eff}}^{12}$) increases abruptly with pressure and is always greater than zero, since the isotropic compression second derivative of the total energy of any crystal grows with decreasing volume. Both the $B1$ and $B2$ phases are stable with respect to isotropic compression. However, the response of the H_{vv} (or c_{eff}^{44}) element to p is very different. The existence of one positive and one negative term makes their mutual balance crucial in determining the sign of its sum. Those configurations with positive values of H_{vv} are minima onto the 2D surface and describe, therefore, thermodynamically stable or metastable crystals. Those with negative values are saddle points and describe thermodynamically unstable systems. The same can be said of the proper elastic constants. Configurations with positive c^{44} are mechanically (energetically) stable or metastable, while those with negative c^{44} correspond to mechanically unstable systems. It is interesting to note that long ago Born[39] proposed a c^{44} mechanical instability to explain the $B1$-$B2$ phase transition.

Figure 3 shows the elastic and effective elastic c^{44} constants of the $B1$ and $B2$ phases as a function of pressure. At zero p, the $B1$ crystal is thermodynamically and mechanically stable, while the $B2$ is not. As pressure increases, the $B2$ system becomes first mechanically stable and then thermodynamically metastable (its G function value is still greater than that of the $B1$ crystal). Eventually, and at a pressure higher than the theoretical thermodynamic transition pressure (around 80 GPa), the $B1$ crystal becomes thermodynamically unstable while the $B2$ phase remains stable up to the greatest pressure studied (300 GPa). The driving force of the transition is, in this picture, seen as a cubic angle instability. We can also understand that it is at least theoretically possible to obtain metastable crystals in one chosen phase in regions where the thermodynamically stable phase is the other
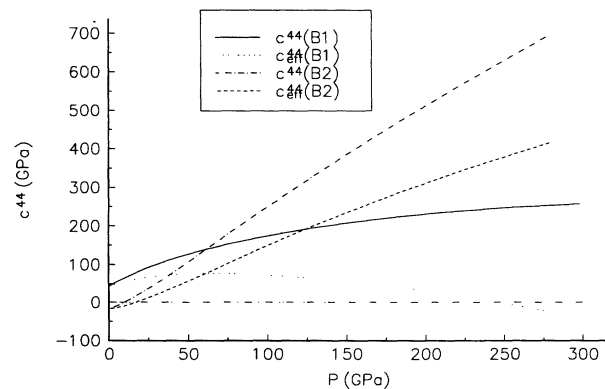

FIG. 3. Elastic and effective elastic constants (c^{44} component) for the $B1$ and $B2$ LiCl crystals as a function of pressure according to AIPI calculations. Both thermodynamic ($c_{\text{eff}}^{44}=0$) and mechanical ($c^{44}=0$) instabilities are patent.

one if, and only if, we are in the inner p region where both c_{eff}^{44} are positive (the stability range). It should not be viable (and hence attempted) to isolate the $B2$ phase at pressures below ~ 20 GPa or the $B1$ phase beyond ~ 250 GPa. We will see in the next section that these two values are indeed the theoretically obtained limits for the hysteresis range at 0 K.

V. TRANSITION PATH AND TRANSITION KINETICS

In Sec. III we showed how the reaction path for our simplest 9D model was really restricted to a 2D surface. After studying the main topological features of this surface and their physical meaning, we turn to the actual determination of the transition path. We define it as the *minimum Gibbs potential path* connecting the end configurations $(B1,B2)$ at each pressure. Since the most representative coordinate of the transition out of the transition configuration space is the rhombohedral angle α, we have chosen it as the reaction coordinate. Figure 4 shows the Gibbs reaction diagram for our model system (LiCl). The G values are referred to the $B1$ configuration for each p to better observe the relative stability of the phases. It is apparent from the plot that both the $B1$ and $B2$ points are always critical points, the second changing from a maximum to a deep minimum on increasing p, and the first one experiencing the reverse transformation. These results may be successfully compared with those encountered in the previous section: for example, the stability range introduced there is nothing but the pressure region in which both structures are local minima (see Fig.
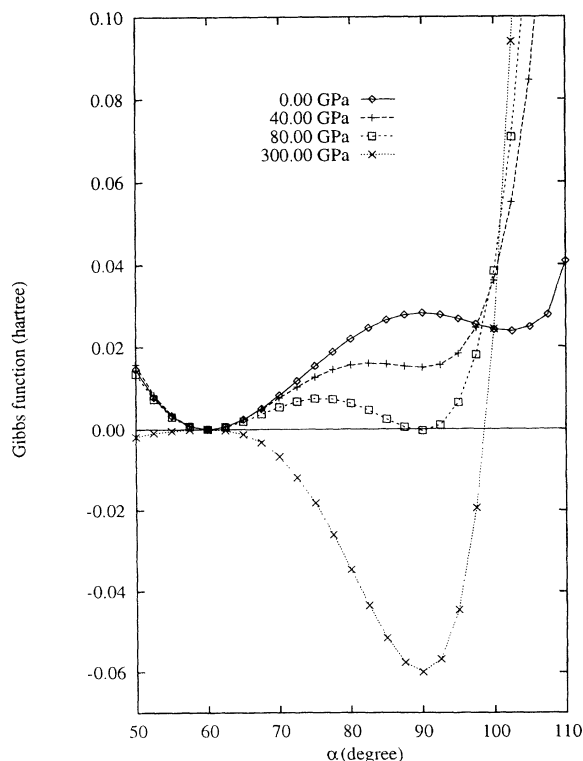
4). The thermodynamic transition pressure is that in which both phases have the same G function value.

Figure 4 gives detailed information about the nuclear process that generates the angle instability. The whole series of transition paths can be interpreted as the movement of a maximum across the angle axis. Whenever it touches one of our end configurations, the latter critical point changes from one type to another. At the moment of this change, one maximum and one minimum coalesce. The process is then catastrophic[40] and one dimensional. The cubic nature of the path in the vicinity of the instability, along with a simple algebraic analysis that we will omit here, allows us to state that the *angle instability is a codimension-1 fold catastrophe.*[40]

It is also crucial to note that stable or metastable $B1$ and $B2$ structures are connected through paths with large barriers, even at pressures well above the thermodynamic transition pressure. This point will be further analyzed, since it lies at the very heart of the hysteresis phenomena.

Figure 5 shows the coupling of the a,α coordinates along the path as a function of pressure. All the curves are practically parallel, so we can say that the a,α coupling does not change in nature with p. The angle starts to open at the $B1$ point while the lattice parameter decreases. Near the $B2$ configuration both movements uncouple each other and at the very $B2$ point the reaction path only changes the cubic angle. As repeatedly encountered in this paper, this behavior is fundamentally symmetry constrained. Since our paths are minimum G paths, the analytical equation of each trajectory in the
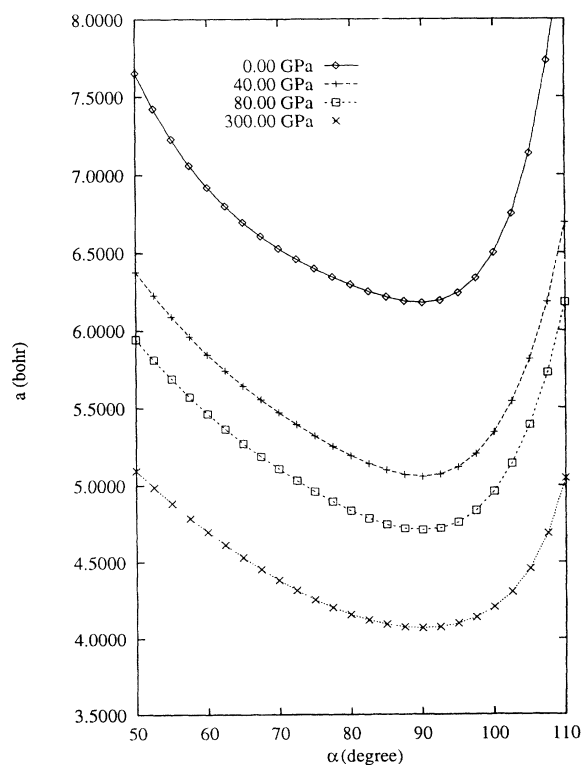
FIG. 4. Theoretical LiCl reaction diagrams onto the 2D 0-K Gibbs surface as a function of pressure.

FIG. 5. a-α coupling along the transition paths as a function of pressure. The slopes of the curves at the $\alpha = 60°$ and $\alpha = 90°$ lines are symmetry determined.

a, α plane is

$$\frac{\partial G(a,\alpha)}{\partial a} = \frac{\partial U(a,\alpha)}{\partial a}$$
$$+ 3pa^2[1 - 3\cos^2(\alpha) + 2\cos^3(\alpha)]^{(1/2)}$$
$$= \frac{\partial U(a,\alpha)}{\partial a} + 3pa^2 f(\alpha) = 0 , \qquad (10)$$

and then the derivative of a with respect to α along the path takes the following expression:

$$\frac{da}{d\alpha} = \left[3pa^2 f'(\alpha) + \frac{\partial^2 U}{\partial a \partial \alpha} \right] \left[\frac{2}{a}\frac{\partial U}{\partial a} - \frac{\partial^2 U}{\partial a^2} \right]^{-1} . \quad (11)$$

At $\alpha = 60°$, and reminding the reader that the crossed U second derivative is zero by symmetry, $da/d\alpha$ is null, no matter the pressure. It is also easy to show, though more cumbersome, that the derivative at the $B1$ position is also constant with pressure. If the slope of the paths are equal and fixed at the two extreme points, the $B1$ and $B2$ ones, there is little room left for diversity.

The kinetics of a solid-solid transformation is difficult to model due to the many factors involved. It is generally assumed that the main two dominant processes are (a) the cooperative transformation of small regions of a given crystal into the thermodynamically stable phase and, (b) the growing of the grains so formed. As we have seen, the first one has a large Gibbs activation energy in the neighborhood of the thermodynamic transition pressure. The grain growing problem is also affected by a barrier coming from the surface Gibbs energy contribution to the total Gibbs potential, and is much more difficult to study theoretically. As commented in the Introduction, there is experimental evidence that for large, very pure crystals the transformation may occur suddenly and simultaneously over the whole crystal volume. In these cases, the relative kinetic significance of grain growing and grain boundary factors is diminished. In order to properly understand the kinetical information embodied in our results, we shall omit grain aspects in the following.

We have obtained the barriers or activation Gibbs energies for the $B1 \rightarrow B2$ and $B2 \rightarrow B1$ processes as a function of pressure. It is to be noticed that (a) $B1 \rightarrow B2$ and $B2 \rightarrow B1$ activation energies are different at a constant p except at the thermodynamic transition pressure. They decrease almost exponentially as p increases for the $B1 \rightarrow B2$ process, doing the opposite for the $B2 \rightarrow B1$ one. (b) Pressures with thermally surmountable $B1 \rightarrow B2$ activation energies are higher than the thermodynamic transition pressure. The contrary occurs for the $B2 \rightarrow B1$ transition.

If, as usually done, we ascribe the meaning of the barriers to energy that the system must possess in order to overcome the saddle point along the path, and take into account that in a solid reaction this energy has to be vibrational (thermal) in nature, we arrive at a consistent picture of the kinetic experimental facts. Since we have not really enough theoretical information to estimate the absolute thermal energy of a crystal from our calculations, we have supposed a simple Debye model. Though

being only a qualitative guess of the authentic thermal energies, it will serve for our purposes here. Let us imagine now a compression-decompression cycle starting from a $B1$ crystal at constant temperature (see Fig. 4). In the first stages of compression the initial system does not have energy enough to change phase until the pressure takes a value quite bigger than the thermodynamic transition pressure. If we take the recently formed $B2$ crystal and decompress, the backward transformation now occurs at a pressure lower than the thermodynamic transition pressure. This is a hysteresis cycle and the intersections of a constant energy (temperature) line with the activation curves define the hysteresis range. It is seen how this hysteresis range decreases abruptly (actually almost exponentially) with increasing T. The transformation is quasireversible only at large temperatures. The enormous $B1 \rightarrow B2$ pressures needed at usual temperatures may be the key to understand why the phase transition has not yet been observed in LiCl.

The appearance of hysteresis cycles may be clarified with a simple master equation model. If we denote n_1 and n_2 the concentration of the $B1$ and $B2$ phases, suppose Boltzmann factors for both the $B1 \rightarrow B2$ and $B2 \rightarrow B1$ processes, and identify time direction with pressure increase direction, we can write

$$\frac{dn_1}{dp} = \omega_1 e^{-\Delta G^*_{B1 \rightarrow B2}/kT} n_1 - \omega_2 e^{-\Delta G^*_{B2 \rightarrow B1}/kT} n_2 , \quad (12)$$

where the numerators of the exponents are the barrier Gibbs energies of both processes and the ω parameters are adjustable constants in this work that will be investigated in the near future. Making use of our theoretical barriers, Eq. (12) is able to describe hysteresis cycles with the following features: (a) the width of the hysteresis cycle decreases quickly as T increases and as the rate of pressure change decreases; (b) once the appropriate p is reached in both directions, the transformation is completed in a very narrow p range. Infinitely slow transformations are reversible and take place at the thermodynamic transition pressure at any temperature.

Though the kinetic model used here is a very simple one and does not take into account properly many important variables involved in the phase transition, we think that the main qualitative and physical aspects of the bulk $B1$-$B2$ phase transition are well described, and shows how an *ab initio* solid-state methodology can help in the understanding of these difficult problems.

VI. CONCLUSIONS AND PERSPECTIVES

We have shown in this paper how a series of models of growing complexity can be hierarchically and systematically constructed in order to study rigorously the thermodynamic and kinetical behavior of the pressure-induced $B1$-$B2$ phase transition in alkali halides. The full analysis of the simplest of these models, the 9D model, has shown how important the adequate treatment of symmetry is to reduce the dimensionality of the interesting regions of the transition configuration space, and how the main topological and physical properties of the energetic and Gibbs surfaces are constrained by this symmetry. These results

point towards a more detailed consideration of the algebraic aspects of the theoretical studies to be made in the future. With the aid of the AIPI scheme and always within the constrained 9D model, the transition has been shown to obey a modified Buerger mechanism. We have also found that its kinetics is closely related to the phase stability problem and that the driving force of the process is a cubic angle thermodynamic instability. This instability is one dimensional and may be seen as a fold catastrophe in Thom's sense.[40] Many of the experimental findings also emerge from the physical model presented.

We also believe that the present study can be used, due to its general scope, to compare results coming from other simulation techniques (molecular dynamics, Monte Carlo, etc.) and tune the many parameters involved in those methods. Perhaps a combined (*ab initio* and pair potential based) strategy to the problem could be the best way to go further. As regards *ab initio* calculations, the astonishing developments in computer speed allow the consideration of greater dimensionality models that will reduce even more the number of plausible mechanisms involved. We are also studying the transition from the point of view of the chemical bond determining the topological aspects of the electronic density in Bader's[41] sense. We expect to find in this way that the transition is accompanied by a sudden change of chemical connectivity at a given point along the transition path and construct a coherent and global outlook of the transformation.

ACKNOWLEDGMENTS

*On leave from the Medical Academy of Sciences of Riga, Riga, Latvia.

[1] R. K. Singh, Phys. Rep. **85**, 259 (1982).

[2] J. C. Slater, Phys. Rev. **23**, 488 (1924).

[3] P. W. Bridgman, *The Physics of High Pressure* (Dover, New York, 1970).

[4] R. Jeanloz, Rev. Mineral. **14**, 389 (1985).

[5] A. Lacam and J. Peyronneau, J. Phys. (Paris) **34**, 1047 (1973).

[6] X. Li and R. Jeanloz, Phys. Rev. B **36**, 474 (1987).

[7] H. Shoji, Z. Kristallogr. **77**, 381 (1931).

[8] J. Buerger, in *Phase Transformation in Solids,* edited by R. Smoluchowski, J. E. Mayers, and W. A. Weyl (Wiley, New York, 1951).

[9] M. Watanabe, M. Tokonami, and N. Morimoto, Acta Crystallogr. A **33**, 292 (1977).

[10] N. V. K. Prabhakar, R. K. Singh, N. K. Gaur, and N. N. Sharma, J. Phys. Condens. Matter **2**, 3455 (1990).

[11] S. Froyen and M. L. Cohen, Phys. Rev. B **6**, 3770 (1984).

[12] R. L. Erikson, L. E. Eory, and C. J. Hostetler, J. Chem. Phys. **99**, 336 (1993).

[13] N. Nakagiri and M. Nomura, J. Phys. Soc. Jpn. **51**, 2412 (1982).

[14] I. Ruff, A. Baranyai, E. Spohr, and K. Heinzinger, J. Chem. Phys. **91**, 3148 (1989).

[15] M. P. Tosi and F. G. Fumi, J. Phys. Chem. Solids **25**, 31 (1964).

[16] Y. A. Nga and C. K. Ong, Phys. Rev. B **46**, 10 547 (1992).

[17] J. M. Recio, E. Francisco, M. Flórez, and A. Martín Pendás, J. Phys. Condens. Matter **5**, 4975 (1993).

[18] V. Luaña and L. Pueyo, Phys. Rev. B **41**, 3800 (1990).

[19] (a) V. Luaña, M. Flórez, E. Francisco, A. Martín Pendás, J. M. Recio, M. Bermejo, and L. Pueyo, in *Cluster Models for Surface and Bulk Phenomena,* edited by G. Pacchioni, P. S. Bagus, and F. Parmigiani, Vol. 283 of *NATO Advanced Study Institute, Series B: Physics* (Plenum, New York, 1992), p. 605; (b) V. Luaña, A. Martín Pendás, J. M. Recio, and E. Francisco, Comput. Phys. Commun. **77**, 107 (1993).

[20] R. McWeeny, Proc. R. Soc. London, Ser. A **253**, 242 (1959).

[21] E. Francisco, A. Martín Pendas, and W. H. Adams, J. Chem. Phys. **97**, 6504 (1992).

[22] W. H. Adams, J. Chem. Phys. **34**, 89 (1961); **37**, 2009 (1962).

[23] T. L. Gilbert, in *Molecular Orbitals in Chemistry, Physics and Biology,* edited by P. O. Löwdin and B. Pullman (Academic, New York, 1964).

[24] C. Pisani, R. Dovesi, and C. Roetti, *Hartree-Fock Ab Initio Treatment of Crystalline Systems,* Vol. 48 of *Lecture Notes in Chemistry* (Springer-Verlag, Berlin, 1988).

[25] E. Clementi and C. Roetti, At. Data Nucl. Data Tables **14**, 177 (1974).

[26] S. J. Chakravorty and E. Clementi, Phys. Rev. A **39**, 2290 (1989), and references therein.

[27] J. M. Recio, A. Martín Pendás, E. Francisco, M. Flórez, and V. Luaña, Phys. Rev. B **48**, 5891 (1993).

[28] P. B. Ghate, Phys. Rev. **139**, 1666 (1965).

[29] *Handbook of Chemistry and Physics,* 60th ed., edited by R. Weast (Chemical Rubber, Boca Raton, 1970).

[30] C. Kittel, *Introduction to Solid State Physics,* 4th ed. (Wiley, New York, 1971).

[31] C. Kittel, *Introduction to Solid State Physics,* 2nd ed. (Wiley, New York, 1957).

[32] A. J. Cohen and R. G. Gordon, Phys. Rev. B **12**, 3228 (1975).

[33] C. Li-Rong and C. Qing-Hu, J. Phys. Condens. Matter **3**, 775 (1991).

[34] W. A. Basset, T. Takahashi, H. K. Mao, and J. S. Weaber, J. Appl. Phys. **39**, 319 (1968).

[35] S. N. Vaidya and G. C. Kennedy, J. Phys. Chem. Solids **32**, 951 (1971).

[36] R. G. Pearson, Theor. Chim. Acta **16**, 107 (1970).

[37] R. F. W. Bader, Can. J. Chem. **40**, 1164 (1962).

[38] D. C. Wallace, *Thermodynamics of Crystals* (Wiley, New York, 1972).

[39] M. Born and K. Huang, *Dynamical Theory of Crystal Lattices* (Oxford University Press, Oxford, 1954).

[40] R. Thom, *Structural Stability and Morphogenesis* (Benjamin, Reading, MA, 1975).

[41] R. F. W. Bader, *Atoms in Molecules* (Oxford University Press, Oxford, 1990).

[42] A. R. West, *Solid State Chemistry and Its Applications* (Wiley, New York, 1984).